Reconstruction of Monthly Mean 700-mb Heights from Surface Data by Reverse Specification

WILLIAM H. KLEIN AND YING DAI

Cooperative Institute for Climate Studies, Department of Meteorology, University of Maryland, College Park, Maryland

(Manuscript received 7 May 1997, in final form 14 October 1997)

ABSTRACT

This paper demonstrates an objective method of computing monthly mean 700-mb height anomalies (H) at 108 grid points in the Western Hemisphere for a 40-yr period as a function of concurrent anomalies of monthly mean sea level pressure (P), at the same 108 points used for H, and monthly mean surface air temperature (T) averaged over 112 areas in North America. The authors applied a forward stepwise program to derive linear multiple regression equations that explained 81% of the variance of H by means of only 3.5 variables, averaged over all months and grid points. The stability of these equations held up well on 6 yr of independent data in terms of explained variance, root-mean-square error, and the spatial anomaly correlation coefficient. Therefore, it seems feasible to reconstruct maps of H for the first half of the twentieth century as a function of data on P and T only.

1. Introduction

The Climate Prediction Center of the National Oceanographic and Atmospheric Administration has been archiving monthly mean 700-mb maps for most of the Northern Hemisphere since 1947. Before that date, reliable and widespread upper-air observations were too limited in both quantity and quality to provide the basis for a good set of analyzed hemispheric maps. As a result, climate researchers do not have available a long series of upper-air maps comparable to either the sea level pressure *Historical Map Series* that goes back to 1899 or the gridded surface air temperature data that go back to 1851 (Jones et al. 1986).

The purpose of this paper is to develop an objective basis for reconstructing a file of monthly mean 700-mb maps that covers approximately the first half of the twentieth century. Such an extension of our archive could contribute to many useful studies of climate and climate change. For example, it would be very valuable to have an accurate file of 700-mb maps for the dust bowl years of the 1930s in the Great Plains of the United States. This would greatly improve our understanding of the relation between extreme weather and the upper-air circulation.

Section 2 summarizes previous attempts to reconstruct upper-air weather maps. Section 3 discusses the data and methodology used in this paper. Section 4 describes a series of experiments leading up to our final specification equations. Section 5 illustrates two sample specification equations and summarizes the climatology of the entire set. Section 6 gives the results of testing the specification equations on independent data by computing three verification statistics. Section 7 concludes the paper by summarizing our main findings and presenting four recommendations for further research.

2. Previous work

Many attempts have been made to compute upper-level pressures (or geopotential heights) from surface data, especially the pioneering efforts of Teisserenc de Bort (1885) and Meisinger (1922). The first systematic attempt to analyze daily historical 10 000-ft (approximately 700 mb) maps for the Northern Hemisphere was made by Willett et al. (1943) for the period from approximately 1924 to 1941. Although all available data were used, emphasis was based on differential analysis from sea level pressure maps of the *Historical Map Series*, assuming normal sea surface temperatures and a moist adiabatic lapse rate over the oceans. Slightly modified and more subjective versions of this method were used by Namias (1944) and the U.S. Weather Bureau (1952).

A completely objective method based on linear multiple regression was developed by Davis and Klein (1945). They first calculated the lapse rate between the surface and 10 000 ft from sea level pressure, surface temperature, and surface wind. They next computed the mean virtual temperature from the lapse rate and surface temperature. Finally, they calculated the 10 000-ft pressure from the mean virtual temperature and sea level

Corresponding author address: Dr. William H. Klein, 5225 Pooks Rd., 929 South, Bethesda, MD 20814.

pressure. Although the method had skill, it was never implemented, perhaps because it was based on single station data only. Consideration of an entire field of potential predictor variables was made possible by the screening techniques of Miller (1958), as applied by Klein et al. (1959). This led to rapid advances in statistical weather prediction, first for 5-day means (Klein 1965), then for daily values (Klein 1967; Klein and Lewis 1970), and finally for monthly means (Klein 1983; Klein and Bloom 1989; Klein and Whistler 1991).

A useful concept called ''specification'' developed from the aforementioned papers. Specification uses screening to compute multiple regression equations for surface weather elements at specific locations and projections as a function of a few concurrent 700-mb heights selected from a large field (also called ''pointwise regression''). The success of this concept in operational weather forecasting indicates that it can be applied to estimate historical 700-mb heights by means of a type of ''reverse specification,'' as suggested by J. Knox (1992, personal communication) and H. Van den Dool (1993, personal communication). A similar technique was applied by Namias (1982, 1986) to specify monthly and seasonal mean 700-mb heights over North America and the northern Pacific from a grid of sea surface temperatures in the extratropical Pacific Ocean.

Finally, it should be noted that Fritts et al. (1971) reconstructed anomalies of sea level pressure, temperature, and precipitation from tree-ring records to estimate seasonal means from 1700 to 1899. Fritts et al. used a multiple regression technique similar to ours but theirs had principal components and canonical correlation instead of pointwise regression based on screening. Recently, Young (1994) reconstructed time series of stream flow in Arizona from monthly precipitation and tree-ring records from 1580 onward.

3. Data and methodology

Our basic data for the predictand (dependent variable) was obtained from the Climate Prediction Center and consisted of the monthly mean 700-mb height anomaly (H) at 108 grid points in the western half of the Northern Hemisphere. We used data on a 10° lat–long grid from 70° to 20°N and 180° to 10°W for the 40-yr period from 1951 to 1990.

Our potential predictors were simultaneous monthly mean anomalies of the following variables: 1) sea level pressure (P) at the same 108 points used for H; 2) surface air temperature (T) and precipitation (p), averaged over 68 climate divisions (CDs) selected from a total of 344, to approximate equal spacing over the contiguous United States; and 3) surface air temperature averaged over 44 boxes of size 5° lat × 5° long in the remaining land areas of the Western Hemisphere (p was not available). Figure 1 shows the central location of each of the 68 CDS, whose temperature and precipitation data were obtained from the National Climate Data Center in Asheville, North Carolina (Cayan et al. 1986), as well as the 44 temperature boxes with data compiled at the University of East Anglia in the United Kingdom (Parker et al. 1994).

In order to develop an objective method of reconstruction, we reversed the customary technique of specifying concurrent values of surface weather elements (such as temperature, precipitation, dewpoint, and wind speed) from H. Instead, we specified H from surface elements that were available before 1951, such as the potential predictors listed in the preceding paragraph. Hence, the expression ''reverse specification'' seems appropriate for this study.

We used a forward stepwise regression procedure (screening) to derive linear multiple regression (specification) equations for H for each month and grid point. In order to increase the stability of our specification equations, we pooled data for each target month with its two adjacent months, thereby increasing our sample size from 40 to 120. For example, the equations for October were derived from data for September, October, and November.

We used an automatic cutoff procedure to select additional terms for the regression equations (IMSL, Inc. 1991), but other subroutines would have produced similar results. We chose critical levels that were inversely related to the number of independent variables offered to the screening program. In this way, we kept the number of variables in the specification equations down to approximately 2–6. This range has been effective in previous screening studies such as Klein and Lewis (1970), Klein and Yang (1986), Klein and Bloom (1989), and Klein and Whistler (1991). The resulting multiple regression equations usually satisfied criteria for statistical stability and synoptic reasoning. Our criterion for goodness of fit was the square of the multiple correlation coefficient (%), which is equivalent to the percent reduction of the unexplained variance or reduction of variance (RV).

4. Derivation of specification equations

In preliminary work, we first experimented with our predictor fields one at a time. Table 1, part a, line 1, shows that the field of sea level pressure reduced the unexplained variance of H by about 74%, averaged over all four seasons of the year and 108 grid points (last column). We used a critical probability level of 1/10 of 1% (0.10%, third column) in order to prevent spurious relations from artificially raising the RV. The screening of P produced higher RV over oceans than over land, as illustrated in Fig. 2, but screening of temperature gave the opposite pattern (not shown). This result can probably be attributed to the fact that the lower troposphere tends to be equivalent barotropic over oceans but baroclinic over continents (Klein 1967).

For the remainder of Table 1, part a, a more lenient critical level was used. Nevertheless, the RVs on lines

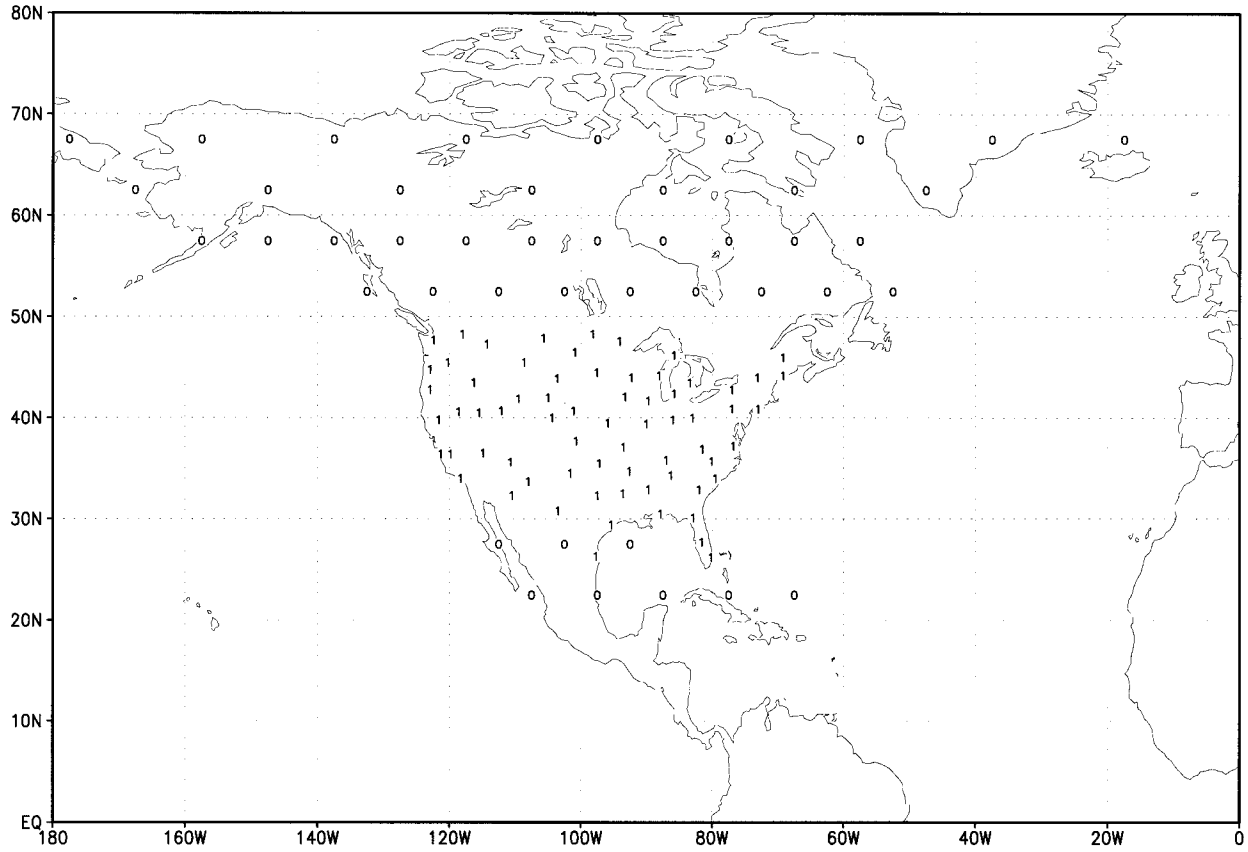

FIG. 1. Location of surface air temperature monthly mean anomalies used as potential predictors for screening. The black vertical symbols are the centers of 68 climate divisions in the contiguous United States. The open ovals show the centers of 44 boxes (5° lat × 5° long) selected to cover most of the remaining land areas of North America and the vicinity.

TABLE 1. Mean values of RV (%) for specification equations giving monthly mean 700-mb height anomalies at 108 points from 70° to 20°N and 180° to 10°W as a function of concurrent anomaly fields of sea level pressure (*P*), surface temperature (*T*), and precipitation (*p*) from 1951 to 1990. The second column shows the number of potential predictors. The third column gives the probability level required for statistical significance.

Predictor	Number of variables	Critical level (%)	Winter	Spring	Summer	Fall	Year
a. Single predictor fields (108 points for *P*, 68 points for *T* and *p* in the United States, and 44 points for *T* in the rest of North America)							
P	108	0.10	80.9	74.7	66.7	72.4	73.7
T	68	5.00	47.7	39.8	33.5	30.9	38.0
T	44	5.00	47.4	44.5	36.7	36.5	41.3
T	112	1.00	52.8	49.3	41.0	39.4	45.6
p	68	5.00	35.4	25.4	25.5	23.3	27.4
b. Two predictor fields (108 *P* points and 112 *T* points)							
P and *T*	220	0.10	87.4	83.7	76.2	81.5	82.2
P and *T*	220	0.05	86.8	83.1	75.1	80.3	81.3
P and *T*	220	0.01	86.0	82.1	72.5	78.9	80.1
P and *T*	220	0.03	86.6	82.4	74.3	80.0	80.8
c. Three predictor fields (108 *P* points, 112 *T* points, and 68 *p* points)							
P, *T*, and *p*	288	0.10	87.5	83.9	76.2	81.5	82.3
P, *T*, and *p*	288	0.05	86.9	83.3	75.2	80.3	81.4
P, *T*, and *p*	288	0.01	86.1	82.1	73.5	78.9	80.2

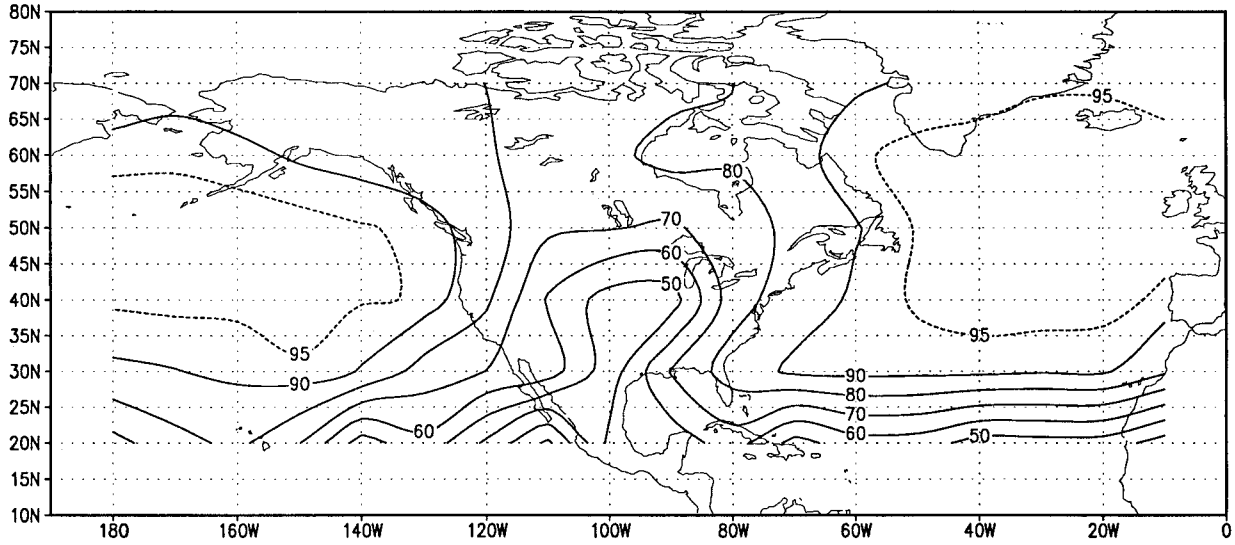

FIG. 2. The percent of variance of *H* explained by screening the field of sea level pressure during winter at a critical probability level of 0.10%. The RV isopleths are drawn at intervals of 10% except for 95%, which is dashed.

2–5 were all considerably less than the 74% for P in line 1. For example, the RV for temperature and for precipitation in the 68 climate divisions of the United States was 38% and 27%, respectively, despite a critical level of 5%. The RV for T in the 44 boxes was 41%, with the same 5% critical level. The surface air temperature (*T*) for the combination of 68 CDS and 44 boxes yielded an RV of 46% at the 1% level. Here the critical level was 1% because the number of independent variables was approximately double the number in lines 2, 3, and 5. It is also noteworthy that the RV was generally highest in winter and lowest in summer or fall.

Part b is similar to part a of Table 1 but for the two predictor fields of 108 points for P and 112 for T. Because of the large number (220) of potential variables, we reduced our critical probability levels drastically over those used in part a. We tried three different values ranging from 0.10% to 0.01% critical levels (third column), corresponding on average to 4.2–3.1 number of variables in the specification equations (not shown). The RVs corresponding to the above values ranged from 82% to 80%, considerably greater than the RV for the single predictors in Table 1, part a.

Table 1, part c, presents the results of adding a third predictor field consisting of precipitation (*p*) at each of the 68 CDs. The improvement in RV produced by adding *p* as a potential predictor was negligible (only 0.1% for each of three critical levels). Therefore, *p* was dropped from further consideration in this study. On the other hand, the addition of temperature to *P* was clearly worthwhile, especially over the continents. On a hemispheric basis, it increased the seasonal RV by 6.5% in the winter and 9.5% in the summer, as shown by comparing the last five columns of parts a and b of Table 1 (line 1). As a result of these and other experiments, we derived final specification equations for *H* based only on *P* and *T*, with a compromise value of 0.03% as the critical probability level (Table 1, part b, line 4). For all months and grid points, the final equations based on this criterion yielded an RV of 81% by means of just 3.5 variables.

TABLE 2. Sample multiple regression statistics obtained by screening monthly mean 700-mb height anomalies from 1951 to 1990 as a function of the concurrent anomaly fields of monthly mean sea level pressure (*P*) and surface air temperature (*T*). The significance level at which a predictor variable was accepted in an equation (cutoff criterion) was 0.03% applied to the reduction of variance (RV) added at each step.

Step	Predictor	Location	Added RV (%)	Cumulative RV (%)	Coefficient in final equation
a. 60°N, 20°W during December, January, and February					
1	*P*	60°N, 20°W	95.40	95.40	5.961
2	*P*	60°N, 10°W	1.90	97.30	3.221
b. 40°N, 100°W during June, July, and August					
1	*T*	42°N, 105°W	50.85	50.85	6.082
2	*P*	30°N, 100°W	18.70	69.55	5.439
3	*P*	60°N, 130°W	5.00	74.55	2.024
4	*T*	29°N, 95°W	2.66	77.21	5.487
5	*T*	53°N, 103°W	4.33	81.54	2.850

5. Properties of final specification equations

Two sample specification equations are illustrated in Table 2. The first is for a point just south of Iceland at 60°N, 20°W during the winter months. Here, only two variables were selected by the screening program. The first was the local sea level pressure *P* (located at the same point as the target point) that explained 95% of the variance of *H*. The second variable (also *P*) added

2% to the RV by including a point at the same latitude as the first point but 10° of longitude due east. The cumulative RV of 97% is remarkably high and equaled only by a point at 50°N in the mid-Pacific Ocean, just south of the Aleutian Islands. This result is consistent with the findings of Klein (1967) working with daily data and the customary type of specification: namely, estimating *P* from *H*. Klein (1967) shows best results near Iceland and the Aleutian Islands, but the RV was considerably lower because of high-frequency meteorological noise in daily data. This indicates that the lower troposphere is strongly equivalent barotropic in east-central parts of the Atlantic and Pacific Oceans.

The second sample equation is for a point at 40°N, 100°W near the center of the United States during summer. Here five variables (three *T*s and two *P*s) made significant contributions to the final RV of *H*. The first variable was the *T* at 42°N, 105°W, located within a few degrees of the target point, which explained 51% of the RV. The second variable was the *P* at 30°N, 100°W, which increased the RV by 19%. The third variable was the *P* at 60°N, 130°W in northwest Canada, which explained an additional 5% of the RV. The last two variables selected by the screening program were both temperatures. The first was located 11° south of the target point and the second 13° to its north. Together they added 7% to the final RV for a cumulative value of 82% in the final equation. The larger number of *T* than *P* variables in this equation and the fact that the first variable selected was a temperature indicate that the lower troposphere tends to be baroclinic over the interior of continents, in sharp contrast to the equivalent barotropic nature of the first sample equation.

The RV, averaged over all 108 specification equations, was computed separately for each month of the year, as illustrated in the upper portion of Fig. 3. The annual cycle is quite smooth, with maximum RV of 87% in winter and minimum RV of 74% in summer, as also indicated in Table 1, part b, line 4. The lower portion of Fig. 3 shows the number of variables selected in the specification equations, averaged over all 108 equations for each month of the year. The curve ranges from a maximum of 3.9 variables in winter to a minimum of 3.2 in summer, and it is roughly parallel to the aforementioned RV cycle. Apparently the strong large-scale weather systems of winter have more significant variables and higher RV than the weak small-scale systems of summer.

The RV as a function of latitude and season is illustrated in Fig. 4. On a latitudinal basis only, the RV was uniformly poor at 20°N but very good (about 90%) from 40° to 70°N. On a seasonal basis, winter had the highest RV at all latitudes and summer had the lowest RV at all latitudes except 60° and 70°N, while the spring and fall seasons were intermediate in RV. When latitude and season were combined (not shown), the RV ranged from 96% at 50°N in January to 33% at 20°N in July.

Figure 5 shows the geographical distribution of RV in winter. The northern three-fourths of this map are surprisingly homogeneous, with RV ranging from above 95% in maritime areas to below 90% in a few parts of the continent. Comparison with Fig. 2, which is based on sea level pressure only and depicts a sharp trough of low RV in the interior of North America, shows that the addition of T as a potential predictor increased the RV over land and reduced the sharp trough over North America to a remnant of lower RV (below 90%). On the other hand, the southern quarter of Fig. 5 contains a very tight gradient of zonally oriented RV isopleths that decrease rapidly from approximately 90% at 30°N to 40% at 20°N. Maps similar to Fig. 5 were prepared for the other three seasons (not shown). Like most features of the general circulation, zonal belts of maximum and minimum RV were farthest north in summer and fall and farthest south in winter and spring.

6. Tests on independent data

In order to test the stability of the specification equations, we used 6 yr of independent data: 4 yr (1947–1950) before our derivation period and 2 yr after it (1991–1992). We then computed three verification statistics: namely, the temporal reduction of variance (RV), the root-mean-square error (rmse), and the spatial anomaly correlation coefficient (*R*).

The first verification statistic was identical to the RV used for the dependent data. We computed the RV for specified values of H at each of our 108 grid points for each month of the year, as before. But now we were limited to a smaller sample (6 yr instead of 40). Table 3 compares the results for both dependent and independent data, averaged over each season and the year as a whole. The last column in Table 3 gives the shrinkage (dependent RV minus independent RV), similar to the ''artificial skill'' discussed by Davis (1976). Reduction of skill is usually expected in testing multiple regression equations, particularly those derived by screening. In this case, however, the shrinkage in going from dependent to independent data was only 2.8% overall.

Like the RV itself, the shrinkage was best (−0.1%) in winter and worst (7.3%) in summer. Likewise, the results of Table 3 show slightly better results in spring than in fall. On a latitudinal basis, averaged over all months (not shown), the shrinkage was 1.2% at 50°N (where the RV was highest) and 4.1% at 20°N (where the RV was lowest). Thus, the RV and its shrinkage were negatively correlated. In addition, the geographical distribution of RV for the independent data closely resembled that of the dependent data (Fig. 5). This provides further evidence that our specification equations are reliable, in part because we limited the selection process to only a few variables in each equation.

Our second verification statistic was based on the same data described for the first statistic, but now we computed the classic rmse instead of the RV used in

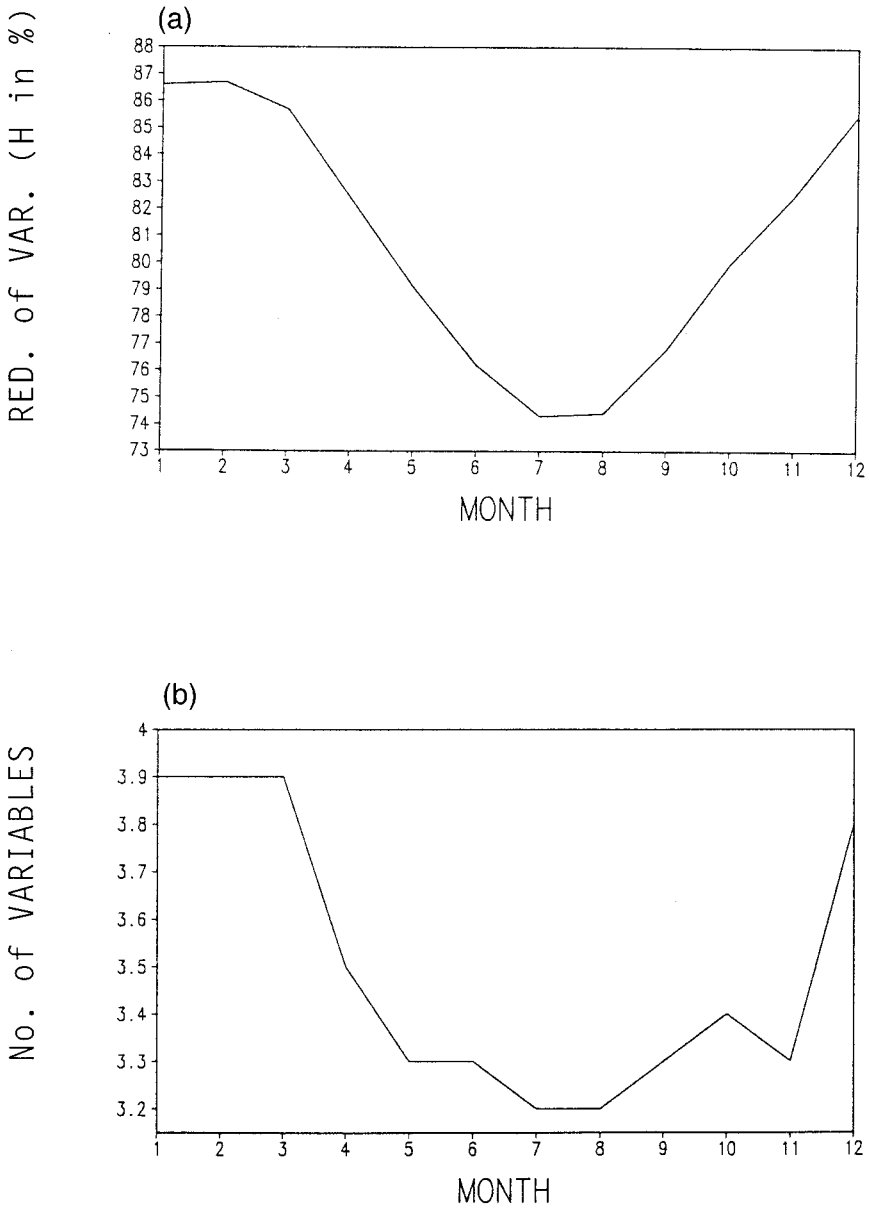

FIG. 3. (a) Annual cycle of reduction of variance of *H* (%) and (b) number of variables in the final specification equations.

Table 3. Table 4 shows that, for all months and grid points, the mean rmse of the specification equations during our 6-yr test period was only 2.7 dam. The range of rmse was small, going from 3.0 dam in winter to 2.4 dam in summer (column 3). In order to provide a reasonable standard for comparison, we computed the mean values of 700-mb height during our 40-yr dependent period (1951–1990), separately for each month and grid point, and assumed them to be the normal heights.

The fourth column of Table 4 shows the rmse obtained by using the normal heights as the best estimate of *H* during our 6-yr test period. The overall rmse was 8.0 dam, an average error approximately three times as large as the 2.7 dam obtained for the specified heights (column 3). The differences in rmse (normal minus specified) was 5.3 dam overall, with range from 8.0 in winter to 3.0 in summer (column 5). On a seasonal and latitudinal basis (not shown), the improvement of specified over normal error ranged from 11.3 dam in winter at 70°N to 0.1 dam in summer at 20°N. It may seem paradoxical that the warmest months and lowest latitudes had the smallest rmse but the least improvement of specified over normal in Table 4. On the other hand, the warmest months and lowest latitudes had the lowest value of RV and largest shrinkage in Table 3. This behavior is probably related to the fact that natural vari-

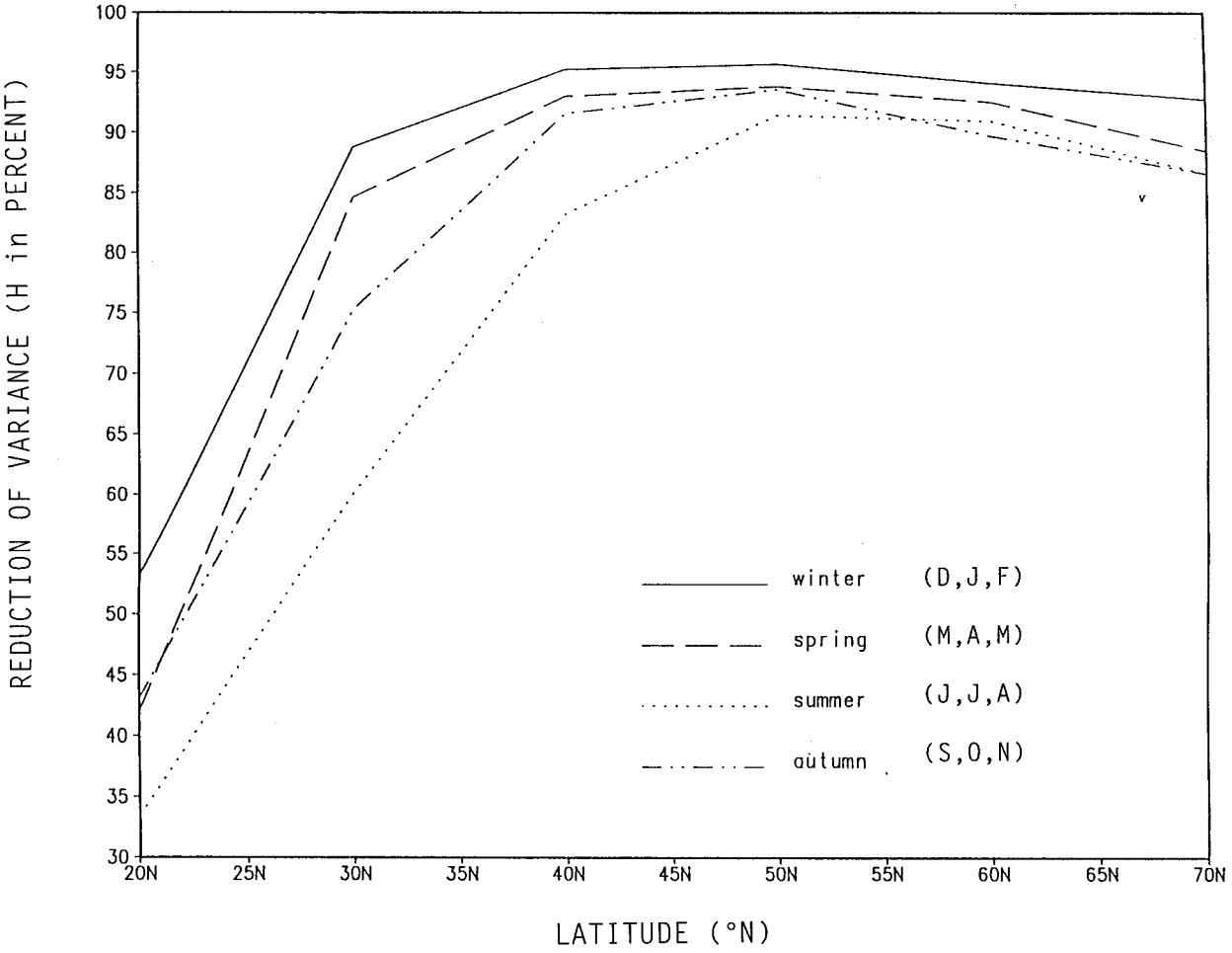

FIG. 4. Reduction of variance H (%) in the final specification equations as a function of latitude and season.

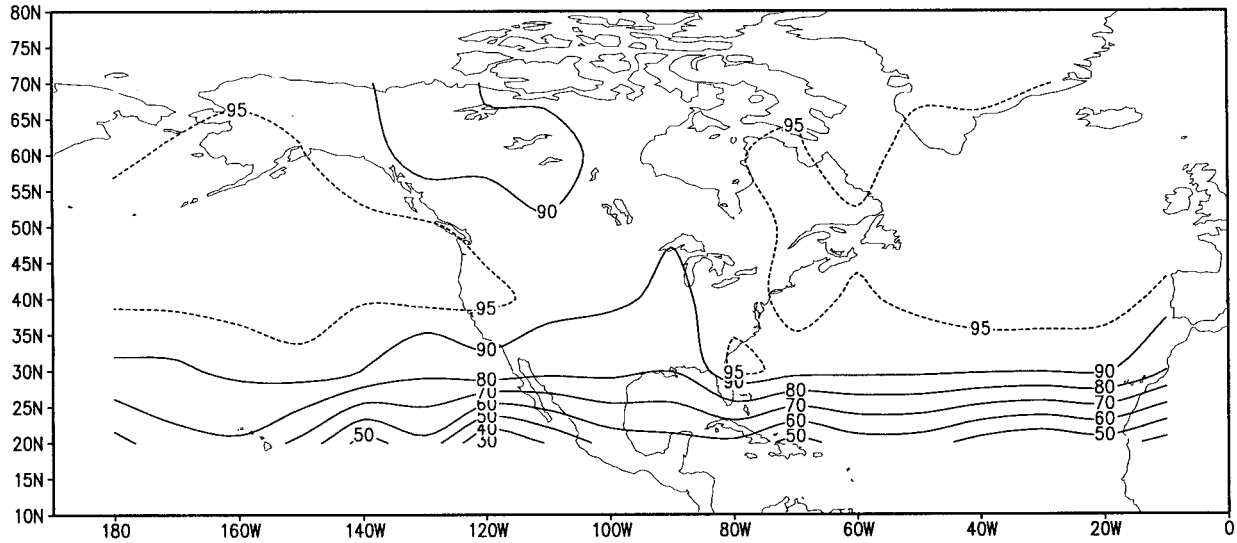

FIG. 5. Geographical distribution of the reduction of variance of H in the final specification equations during winter. The RV isopleths are drawn at intervals of 10% except for 95%, which is dashed.

TABLE 3. Mean temporal values of reduction of variance (%) for specified monthly mean 700-mb height anomalies at 108 points in the Western Hemisphere for independent data (I; 1947–50 and 1991–92) and dependent data (D; 1951–90).

Months	Independent data	Dependent data	Shrinkage (D–I)
Dec, Jan, Feb	86.7	86.6	−0.1
Mar, Apr, May	81.2	82.4	1.2
Jun, Jul, Aug	67.0	74.3	7.3
Sep, Oct, Nov	77.2	80.0	2.8
Year	78.0	80.8	2.8

TABLE 4. Root-mean-square errors (dam) in the Western Hemisphere for specified (S) and normal (N; 40-yr mean) 700-mb height fields during 72 independent months of six test years (1947–50 and 1991–92).

Season	Months	Specified heights	Normal heights	Difference (N − S)
Winter	Dec, Jan, Feb	3	11	8
Spring	Mar, Apr, May	2.6	8	5.4
Summer	Jun, Jul, Aug	2.4	5.4	3
Fall	Sep, Oct, Nov	2.6	7.4	4.8
Year	All 12 months	2.65	7.95	5.3

ability of both *H* and *P* is very small in summer and low latitudes, in contrast to large variability in winter and high latitudes (Klein 1967).

The third verification statistic was the spatial anomaly correlation coefficient (*R*). Unlike the first two temporal statistics with data obtained from time series at each grid point, *R* was computed separately for each individual month and year. It was calculated by comparing the specified with the observed values of H at each of the 108 grid points for each map of the 72 test months (6 yr × 12 months). Table 5 shows that *R*(%) averaged 93.2 for all 72 maps (column 3). On a seasonal basis, the mean *R* ranged from a maximum of 96.0 during the winter months to a minimum of 90.7 in summer. Column 4 gives the range of individual values of *R* by season. The largest range was 0.14 in spring and summer, and the smallest was 0.05 in winter.

In order to show the appearance of the reconstructed maps, we have selected two extremes for comparison with their observed maps. Figure 6 illustrates the best individual reconstruction: namely, the map for February 1992 with an *R* of 98.0. The worst reconstruction was the map for August 1948, when the value of *R* was only 81.0 (Fig. 7). In both cases, however, the specified and observed maps were so similar that it is hard to tell one from the other. This is strong evidence that realistic maps of *H* can be reconstructed from surface data only.

7. Conclusions

We have developed an objective method of computing monthly mean 700-mb height anomalies (*H*) at 108 grid points (70°–20°N and 180°–10°W) for a 40-yr period (1951–90) from concurrent anomalies of monthly mean sea level pressure at the same points used for *H* and monthly mean surface air temperature averaged over 112 areas in North America and the vicinity. We applied a forward stepwise program to derive linear multiple regression equations that explained 81% of the variance of *H* by means of only 3.5 variables, averaged over all months and grid points. The stability of these equations held up well on 6 yr of independent data (1947–50 and 1991–92) in terms of explained variance, root-mean-square error, and the spatial anomaly correlation coefficient. We conclude that it is feasible to reconstruct maps of *H* for the first half of the twentieth century from sea level pressure and surface air temperature only.

A reviewer has questioned the possibility of bias in our estimate of *H*. We therefore compared each set of reconstructed and observed maps by visual examination for all 72 independent cases (as in Figs. 6 and 7). We then assigned each map set into one of three categories: underestimation as in Fig. 6, overestimation as in Fig. 7, and approximately neutral. The results were that 40% of all cases were underestimated, 26% overestimated, and 34% neutral. Thus, the reconstructed maps showed a small bias to underestimate. This bias is to be expected in regression equations based on imperfect correlations, and the bias will increase as the correlation decreases.

Our recommendations for further research are as follows.

1) Rederive the specification equations by using the surface temperature data in 5° boxes (Parker et al. 1994) over the contiguous United States where we previously used climate division data (Cayan et al. 1986). Although the two types of temperature are similar, the first has the advantage of starting in 1851, while the second is neither homogeneous nor conveniently available prior to 1931.
2) Screen the field of sea surface temperature [which goes back to 1854 (e.g., Wolter 1997)] in addition to the fields of sea level pressure and surface air temperature used in this paper. This step may improve our specification equations, especially in summer months at latitudes below 30°N, where our results were very poor.
3) Derive specification equations in the Eastern Hemisphere, using the method of this paper plus the first

TABLE 5. Spatial correlation coefficients for the Western Hemisphere between specified and observed monthly mean 700-mb anomaly fields during 72 independent months of six test years (1947–50 and 1991–92).

Season	Months	Mean R (%)	Range of R (%)
Winter	Dec, Jan, Feb	96.0	93–98
Spring	Mar, Apr, May	93.2	83–97
Summer	Jun, Jul, Aug	90.7	81–95
Fall	Sep, Oct, Nov	92.9	87–96
Year	All 12 months	93.2	81–98

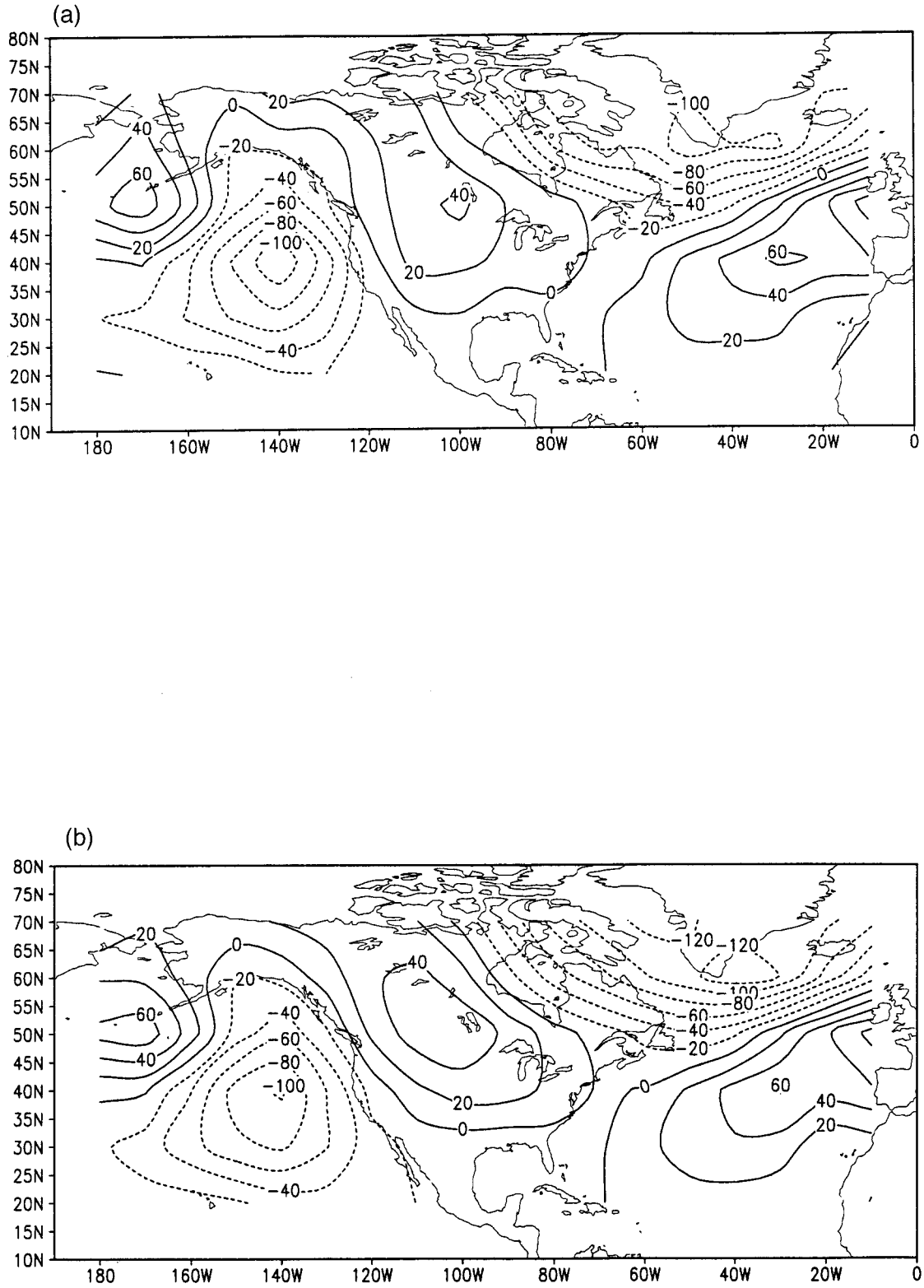

FIG. 6. (a) Reconstructed and (b) observed 700-mb height anomalies for February 1992. The spatial correlation coefficient between the two maps is 0.98, the highest for any of our 72 test months. The isopleths of equal anomaly are drawn at intervals of 20 m, with positive anomalies solid and negative anomalies dotted.

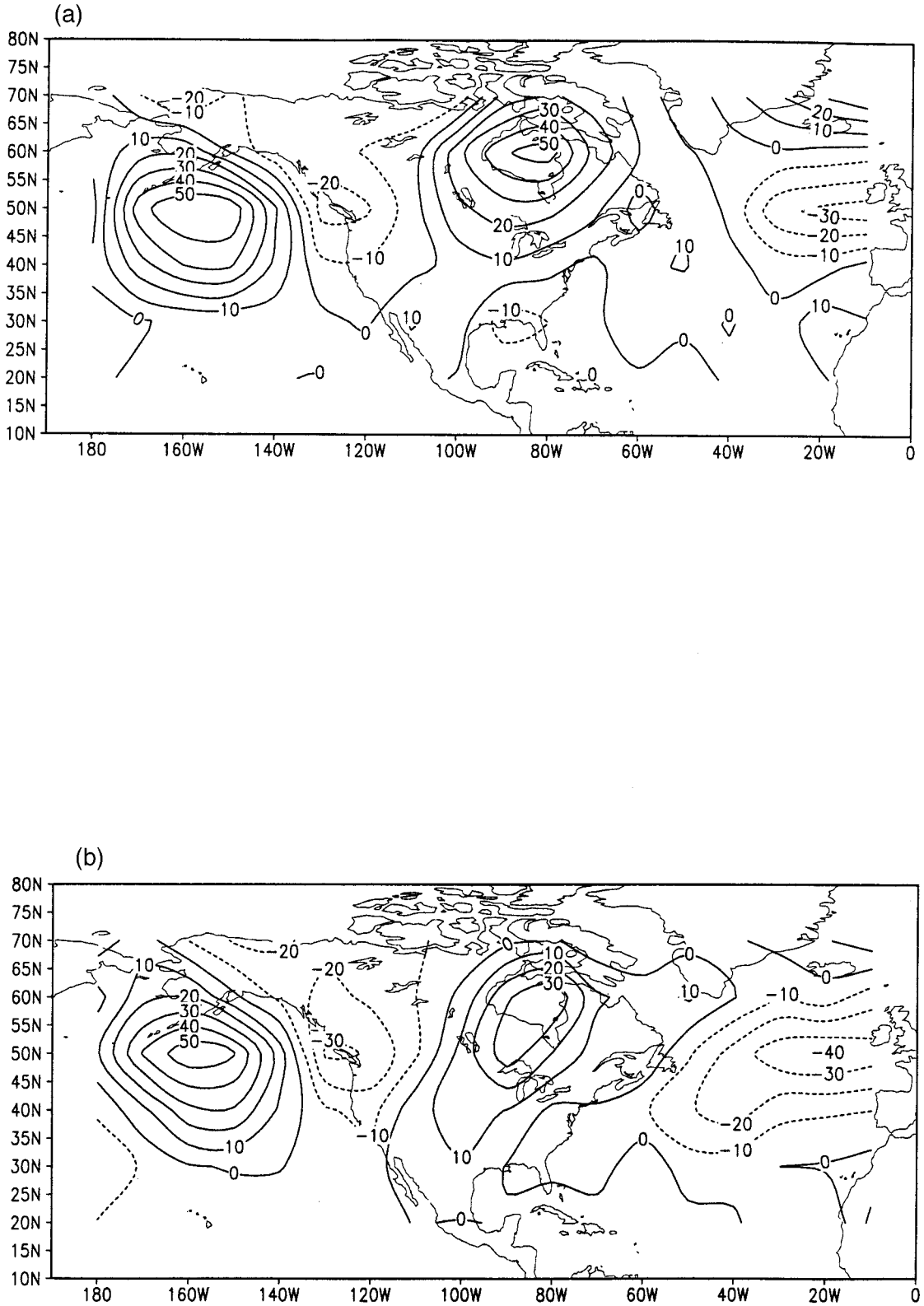

FIG. 7. The same as Fig. 6 but for August 1948 with isopleths at 10-m intervals. The correlation coefficient of 0.81 is the poorest reconstruction of any of our 72 test months.

two recommendations above. However, some data may be limited in mountainous and desert areas.

4) Apply the revised specification equations derived above to reconstruct maps of monthly mean 700-mb height anomalies covering most of the Northern Hemisphere and going back to 1899. This was the first year selected by the U.S. Weather Bureau and Air Force during World War II for their analysis of sea level pressure in the *Historical Map Series.* The combination of this pressure data, the box temperature data listed in recommendation 1, and the sea surface temperatures should provide ideal input into the new specification equations for reconstructing historical upper-air maps.

Acknowledgments. This project was sponsored by the Climate Prediction Center, National Centers for Environmental Prediction, National Weather Service. The research was originally suggested by Huug Van den Dool of the United States' Climate Prediction Center and John Knox of the Canadian Climate Center. Valuable help was received from Tony Barnston and Jin Huang of the Climate Prediction Center, as well as Alan Robock and Jianping Mao of the Department of Meteorology at the University of Maryland.

REFERENCES

Cayan, D. R., C. F. Ropelewski, and T. R. Karl, 1986: *An Atlas of United States Monthly and Seasonal Temperature Anomalies: December 1930–November 1984.* United States Climate Program Office, Department of Commerce, 244 pp.

Davis, F. K., and W. H. Klein, 1945: Computing 10,000-foot pressure from surface data. *Bull. Amer. Meteor. Soc.,* **26,** 147–152.

Davis, R., 1976: Predictability of sea surface temperature and sea level pressure anomalies over the North Pacific Ocean. *J. Phys. Oceanogr.,* **6,** 249–266.

Fritts, H. C., T. J. Blasing, B. P. Hoyden, and J. E. Kutzbach, 1971: Multivariate techniques for specifying tree growth and climatic relationships and for reconstructing anomalies in paleoclimate. *J. Appl. Meteor.,* **10,** 845–864.

IMSL, Inc., 1991: User's manual: Fortran subroutines for statistical analysis, Version 2.0. IMSL, 235–250. [Available from IMSL, Inc., Permian Tower, 2500 City West Blvd., Houston, TX 77042.]

Jones, P. D., S. C. B. Raper, R. S. Bradley, H. F. Diaz, P. M. Kelly, and T. M. L. Wigley, 1986: Northern Hemisphere surface air temperature variations: 1851–1954. *J. Climate Appl. Meteor.,* **25,** 161–179.

Klein, W. H., 1965: Application of synoptic climatology and short-range numerical prediction to five-day forecasting. U.S. Weather Bureau Research Paper, Vol. 46, 109 pp.

——, 1967: Specification of sea level pressure from 700 mb height. *Quart. J. Roy. Meteor. Soc.,* **93,** 214–226.

——, 1983: Objective specification of monthly mean surface temperature from mean 700 mb heights in winter. *Mon. Wea. Rev.,* **111,** 673–691.

——, and F. Lewis, 1970: Computer forecasts of maximum and minimum temperatures. *J. Appl. Meteor.,* **9,** 350–359.

——, and R. Yang, 1986: Specification of monthly mean surface temperature anomalies in Europe and Asia from concurrent 700 mb monthly mean height anomalies over the northern hemisphere. *J. Climatol.,* **6,** 463–484.

——, and H. J. Bloom, 1989: An operational system for specifying monthly precipitation amounts over the United States from the field of concurrent mean 700 mb heights. *Wea. Forecasting,* **4,** 51–60.

——, and B. T. Whistler, 1991: Specification of monthly mean anomalies of fire-weather elements in the United States. *Agric. For. Meteor.,* **56,** 145–172.

——, B. M. Lewis, and I. Enger, 1959: Objective prediction of five-day mean temperatures during winter. *J. Meteor.,* **16,** 672–682.

Meisinger, C. L., 1922: The preparation and significance of free air pressure maps for the central and eastern United States. *Mon. Wea. Rev.,* **50,** 453–468.

Miller, R. G., 1958: The screening procedure. A statistical procedure for screening predictors in multiple regression. *Studies in Statistical Weather Prediction,* Part II, Travelers Weather Research Center, 86–136.

Namias, J., 1944: Construction of 10,000-foot pressure charts over ocean areas. *Bull. Amer. Meteor. Soc.,* **25,** 175–182.

——, 1982: Sea surface temperature teleconnections in the North Pacific and related coastal phenomena. Preprints, *First Int. Conf. on Meteorology and Air/Sea Interaction of the Coastal Zone,* The Hague, the Netherlands, Amer. Meteor. Soc., 286–289.

——, 1986: Autobiography. *Namias Symposium,* J. O. Roads, Ed., Scripps Institution of Oceanography Reference Series 86-17, 30–36.

Parker, D. E., P. D. Jones, C. K. Folland, and A. Bevan, 1994: Interdecadal changes of surface temperature since the late nineteenth century. *J. Geophys. Res.,* **99,** 14 373–14 399.

Teisserenc de Bort, L., 1885: Étude sur la circulation général de l'atmosphére. *Annales du Bureau Central Meteorologique de France, Part IV,* 35–44.

U.S. Weather Bureau, 1952: Normal weather charts for the Northern Hemisphere. Weather Bureau Tech. Paper 21, 74 pp.

Willett, H. C., W. H. Klein, and F. K. Davis, 1943: Historical daily 10,000 ft. maps for the Northern Hemisphere. U.S. Air Force Project.

Wolter, K., 1997: Trimming problems and remedies in COADS. *J. Climate,* **10,** 1980–1997.

Young, K. C., 1994: Reconstructing streamflow time series in central Arizona using monthly precipitation and tree ring records. *J. Climate,* **7,** 361–374.